UC Santa Cruz

UC Santa Cruz Previously Published Works

Title

Solid-state membranes formed on natural menisci.

Permalink

https://escholarship.org/uc/item/3dn1k422

Journal

Nanotechnology, 31(44)

Authors

Walker, Zach

Wells, Tanner

Lay, Kalliyan

et al.

Publication Date

2020-10-30

DOI

10.1088/1361-6528/aba711

Peer reviewed

Solid-state membranes formed on natural menisci

Zach Walker[1], **Tanner Wells**[1], **Kalliyan Lay**[1], **Mohammad Julker Neyen Sampad**[2], **Holger Schmidt**[2], **Aaron Hawkins**[1]

[1]Department of Electrical and Computer Engineering, Brigham Young University, Provo, UT, United States of America

[2]School of Engineering, University of California, Santa Cruz, CA, United States of America

Abstract

We present a method to create robust, nanoscale solid-state membranes using the natural shape of a liquid meniscus as a template. A narrow, open channel is etched into a silicon substrate and then a photoresist polymer is introduced into the channel through spontaneous capillary action. The natural concave meniscus formed by the polymer is then covered by a thin chemical vapor deposited membrane. The polymer is removed by sacrificial etching, leaving behind a suspended membrane. Membranes as large as 20 μm by 9 mm can be fabricated with a thickness as low as 50 nm.

Keywords

microfabrication; microfluidics; biosensors; nanopores; membrane

1. Introduction

Synthetic membranes are a crucial part of many microelectronic devices and have become commonplace in a variety of microelectromechanical systems and microfluidic applications. Pressure sensors [1], resonant sensors [2], thermal actuators [3], ion-sensitive field-effect transistors [4], micromirrors [5], and microfluidic pumps [6] rely on membrane motion. Exciting applications such as biomolecular analysis using nanopores formed within membranes [7] and other biosensors [8] rely on membranes as molecular gates and filters, often mimicking structures and processes found in nature.

Construction of membranes with nanoscale thicknesses has been a challenge, especially for membranes intended to be interfaced with microscale elements like fluid channels, optical waveguides, or electronic circuitry. Robust silicon-nitride nanoscale membranes can be made using bulk micromachining through a silicon substrate, but this process is best used for isolated membranes [9]. More readily integrated surface micromachining that attempts to stretch membranes over sacrificial regions has suffered from abrupt edges at interfaces between materials [10]. These non-continuous boundaries, even when different by only nanometers, create stress and cracking in overlaid membranes.

hawkins@ee.byu.edu.

Our design highlights the robust nature of a membrane fabricated on a smooth surface formed by a natural meniscus. Such a meniscus can be created without an abrupt step at material interfaces. In our demonstration, we used a photoresist polymer, SU8-2000.5, to form a liquid meniscus in a narrow trench etched between two fluid reservoirs. The SU8 naturally flows into the microfluidic channels by way of the spontaneous capillary effect [9–11] and fills the entire trench up to the edge of the channel wall. The boundary of the meniscus is perfectly pinned at this edge and takes on a smooth concave shape. Once the polymer is hardened by an elevated temperature, a SiO_2 membrane is grown on top of the SU8-2000.5 using plasma-enhanced chemical vapor deposition (PECVD), and the SU8 is sacrificially removed, leaving the thin membrane straddled across the width of the hollow trench.

The dimensions of the nano-membrane can be tailored to fit a variety of designs. As shown in our experiments, membrane widths can vary from 2 to 25 μm and the depth of the underlying trench can range from 4 to 20 μm. The overall length of the membrane depends upon the depth of the trench, but for our choice of materials, varied between 4 and 8 mm. Tests were done to show that SiO_2 membranes can be fabricated as thin as 50 nm and still remain intact and durable. Given the adjustable aspect ratio, the channel cross-sectional area can be shaped according to a given application.

2.   Nanofabrication process

As illustrated in figure 1, our nanofabrication process utilizes many of the well-known techniques from the microelectronics industry. Features were first patterned onto a 100 mm silicon wafer using photolithography and AZ Nlof 2020 photoresist (figure 1(a)). Designs patterned on the wafer included narrow trenches connected to large, circular 'reservoirs' at both ends. Trench widths ranged from 2 μm to 25 μm and were 8 mm long. An STS ICP Multiplex ASE was used for anisotropic etching into the silicon. Etch depth was varied between 4 and 20 μm on different wafers.

After etching, the resist mask is removed with acid and then wafers were placed into a furnace where a 200 nm layer of thermal oxide was grown (figure 1(b)). This oxide layer provides a thin electrically insulating layer along the trench walls and also allows for better capillary flow in the subsequent processing step. SU8-2000.5 was manually placed in the reservoirs at both ends of the 8 mm long channels. Once dropped into the reservoir, it begins to flow into the channels due to capillary action and forms a sacrificial layer inside the trenches (figure 1(c)). SU8-2000.5 was chosen due to its low viscosity and ability to flow easily in the trenches. The flow process was aided by placing the wafer on a hotplate and ramping the temperature to 250 °C. The higher temperature allows the SU8-2000.5 to flow further down the trenches, extending the subsequent channel and membrane length. The higher temperature also allows the SU8-2000.5 to harden after it has flowed (figure 1(d)).

PECVD silicon dioxide was then grown over the wafer (figure 1(d)) using in an Oxford Instruments machine with a mixture of SiH_4/Ar and N_2O gas at 250 °C. The thickness of the SiO_2 membrane was a critical parameter in our design process. 200 nm, 150 nm, 100 nm and 50 nm thick films were tested. Finally, the wafers were placed in a mixture of H_2O_2 and

H_2SO_4 to remove the sacrificial SU8-2000.5 [10]. The result is a hollow microfluidic channel covered by an ultra-thin membrane. The dimensions of the channel can vary significantly and still produce robust, thin membranes.

3. Utilizing the capillary effect

The most interesting aspect of our nanofabrication process is the capillary filling technique. The spontaneous capillary flow of SU-8 2000.5 produces a natural profile with an upper concave meniscus [11]. A number of surface effects contribute to capillary flow, including surface tension. Surface tension is defined as Gibbs free energy per area for fixed pressure and temperature [12] and is highly dependent on the materials involved. Higher surface tension allows for greater adhesion of the fluid molecules to the substrate and overall capillary flow [13]. Raising the temperature in our process increases surface tension and thus increases the SU8 capillary flow length [14].

Another important surface effect observed in our devices is that the SU8 will climb up the channel walls but will not spill over. Since SU8 is a solution with a polar solvent, the hydrophilic SiO_2 walls allow the SU8 to climb to the top of the channel where it forms a concave meniscus. The angle of the concave meniscus shaped by the SU8 on the wall of the channel is known as the contact angle [15]. This is shown in Young's equation for contact angle as shown below

$$cos\theta = \frac{\gamma_{sg} - \gamma_{sl}}{\gamma_{lg}} \tag{1}$$

where θ is the contact angle, γ_{sg} is the surface tension between the SiO_2 and air, γ_{sl} is the surface tension between the SiO_2 and SU8 and γ_{lg} is the surface tension between SU8 and air [15].

Figure 2 shows scanning electron microscope (SEM) images of completed membranes made using our process. These images were made by cleaving the underlying silicon substrate orthogonally through the microchannels and 200 nm thick membranes. Under the membranes are hollow channels that are 3 μm wide and 7 μm wide respectively. Both channels are 12 microns deep. In both cases, the membrane is uniform and intact. The wider membrane looks flatter and indeed drops less into the underlying channel at its center point.

The shape of the meniscus created due to capillary flow can be described in its simplest form using a circular model. This model is typical for a liquid meniscus under the capillary effect [16]. In narrower channels, two circularly shaped regions would meet at a point in the middle of the channel. In wider channels, there would be a flat section at the bottom of the meniscus between two circular regions.

The radius of curvature of the circular region is a property of the liquid-substrate contact angle which generally does not change with varying channel widths. In our case, the meniscus meets the channel wall at the top of the channel, where there is a corner in the substrate as shown in figure 3.

Because of this corner, the contact angle can vary and generally increases with larger channel width according to the measurements shown in figure 4 as well as reported by other researchers [13, 17, 18]. Based on our model and the measured contact angle, predicted meniscus depths can be calculated. Figure 4(a) shows these predicted meniscus depth values and plots them against measured meniscus depths. The variation in contact angle not only changes the meniscus depth but also the shape of the meniscus. The profile of the meniscus for varying channel widths based on our simple circular model is shown in figure 4(b). The widths and contact angles used for this figure were measured from a set of sample channels. As figure 4 illustrates, the meniscus depth decreases for wider channels because of the changing contact angle of the meniscus with the channel wall, which is consistent with observations.

4.   Membrane size and robustness

The thickness, length, and width of the membrane were parameters that varied in order to determine the range of achievable dimensions. The etch depth of the channel trenches also proved to be an important parameter and directly correlated to the capillary flow distance of the SU8-2000.5 and thus the overall length of the membrane.

The length of the channel and membrane are first considered. When dropping SU8-2000.5 into the channel reservoirs at room temperature, the SU8-2000.5 would only flow into the trench a short distance (typically 2 mm or less depending on the depth of the channel). When exposed to heat, the SU8-2000.5 flows significantly further due to the increase in the surface energy. Higher and lower temperatures were tested but the longest SU8 flow distance occurred at 250 °C. In our design, there are reservoirs on either side of each channel which allows the SU8-2000.5 to flow from both sides and connect in the middle. If the SU8-2000.5 does not connect in the middle, a gap will be produced where no membrane is formed.

Another consideration regarding the overall flow distance was the thermal oxide grown in the furnace before the SU8-2000.5 was placed in the reservoirs. The presence of thermal oxide in the channel instead of bare silicon did help the SU8-2000.5 to flow further due to higher surface energy of the silicon dioxide as compared to silicon.

A major factor that affected the flow distance of the SU8-2000.5 was the etch depth of the microfluidic channels as shown in figure 5. The channel depths tested were 4, 8, 12, and 20 μm. The trend in figure 5 shows the deeper the channel was etched, the further the SU8-2000.5 flowed. Figure 5 also shows how the channel width affects the overall flow length of the SU8-2000.5. In general, the wider channels allowed the SU8-2000.5 to flow further.

The width and depth of the channels as well as the membrane thickness were important factors that helped determine the overall yield. These parameters were varied in order to provide a comprehensive test as to which geometries allow for the most reliable membrane fabrication process. Figure 6 demonstrates the percent yield of the membrane for a given channel width, depth and membrane thickness. Ten membrane widths were tested between 2 and 25 μm. Various membrane thicknesses were also tested in order to determine how thin

membranes could be made using our fabrication process. Four thicknesses were tested; 200, 150, 100 and 50 nm. The 4, 7, 12, and 20 μm wide channels were found to be representative of the different widths tested and the results for these channels are summarized in figure 6.

Results from figure 6 were obtained by fabricating channels with the designated width, height, and membrane thickness. The channels were marked and divided into sections. The length of broken and intact sections of each individual channel were measured with an optically with a microscope. The percent yield was then calculated as the percentage of intact sections with respect to the given channel length. Only the sections of the channel where SU8 had flowed were considered in the percent yield calculations so the membrane lengths used for the percent yield calculations varied from channel to channel. Each test was performed on five different channels of the same width, height and thickness in order to obtain an average percent yield as represented in figure 6.

Figure 6 demonstrates that thicker membranes tend to create more robust membranes and resulted in higher percent yields. 200 nm thick membranes achieved high percent yields for many different widths and depths unlike the 50 nm thick membranes that did not hold up well in many cases. Another conclusion from figure 6 is that deeper channels result in lower percent yields. However, as shown in figure 5, increasing the depth results in longer channels and membranes because capillary flow increases with channel depth. One optimal case was the 7 μm wide, 12 μm deep channel with 200 μm thick membranes. It resulted in 100% yield and flowed over 5 mm making for a long, robust membrane. The 7 μm by 12 μm dimensions also allows for a sufficient volume to be carried in the channel for a variety of applications.

For channels that did not have a high yield percentage, the two main issues observed were highly stressed membranes and membranes that were not strong enough to span the width of a given channel. The membranes with high amounts of stress would become weak in certain areas and would collapse in on themselves.

5. Conclusion

By way of the spontaneous capillary effect, thin silicon dioxide membranes were fabricated on a natural meniscus formed by SU8-2000.5. The membranes were constructed for a variety of different channel widths, lengths and membrane thicknesses. The fabrication process for designing these membranes has proven to be robust and can create strong membranes that can be used for a variety of different applications. Given the high percent yield for many of the membranes tested, channel dimensions can be widely varied to fit a variety of design criteria.

Acknowledgments

References

[1]. Chen M, Luo W, Xu Z, Zhang X, Xie B, Wang G and Han M 2019 An ultrahigh resolution pressure sensor based on percolative metal nanoparticle arrays Nat. Commun10 4024 [PubMed: 31492843]

[2]. Adiyan U, Larsen T, Zárate JJ, Villanueva LG and Shea H 2019 Shape memory polymer resonators as highly sensitive uncooled infrared detectors Nat. Commun 10 4518 [PubMed: 31586068]

[3]. Lake RA, et al. 2014 Thermal tuning of MEMS buckled membrane actuator stiffness Science Direct (10.1016/j.proeng.2014.11.700)

[4]. Jimenez-Jorquera C et al. 2010 ISFET based microsensors for environmental monitoring Sensors 10 MDPI 61–83 [PubMed: 22315527]

[5]. Werber A and Zappe H 2006 Tunable, membrane-based, pneumatic micro-mirrors J. Optics 8 S313–4

[6]. Kim H, Kim K and Lee S 2016 Compact and thermosensitive nature-inspired micropump Sci. Rep 6 36085 [PubMed: 27796357]

[7]. Liu S, Hawkins AR and Schmidt H 2016 Optofluidic devices with integrated solidstate nanopores Microchim. Acta 183 1275–87

[8]. Hurk R et al. 2015 A review of membrane-based biosensors for pathogen detection Sensors 15 14045–78 [PubMed: 26083229]

[9]. Dücsö C, Vázsonyi É, Ádám M, Bársony I, Gardeniers JGE and Van Den Berg A 1997 Porous silicon bulk micromachining for thermally isolated membrane formation Sensors Actuators A 60 235–9

[10]. Holmes MR 2011 Integration of micropore and nanopore features with optofluidic waveguides for single particle sensing Brigham Young University - Provo. Scholars Archive pp 2572–4479

[11]. Berthier J, Brakke KA, Gosselin D, Navarro F, Belgacem N and Chaussy D 2016 Spontaneous capillary flow in curved, open microchannels Microfluid. Nanofluid 20 100

[12]. Calvimontes A. 2017; The measurement of the surface energy of solids using a laboratory drop tower. Npj Microgravity. 3:25. [PubMed: 29046893]

[13]. Seemann R, Brinkmann M, Kramer EJ, Lange FF and Lipowsky R 2005 Wetting morphologies at microstructured surfaces Proc. Natl Acad. Sci 102 1848–52 [PubMed: 15677720]

[14]. Sou ková M et al. 2008 Measurement and correlation of the surface tension-temperature relation for methanol J. Chem. Eng. Data ACS Publications 53 2233–6

[15]. Jiang H, Müller-Plathe F and Panagiotopoulos AZ 2017 Contact angles from Young's equation in molecular dynamics simulations J. Chem. Phys 147 084708 [PubMed: 28863512]

[16]. Jasvanth VS et al. 2019 Numerical investigation of an evaporating meniscus in a heated capillary slot Heat Mass Transfer 55 3675–88

[17]. Wijs W-J, Laven J and With G 2016 Wetting forces and meniscus pinning at geometrical edges AIChE J 62 4455

[18]. Sowers TW, Sarkar R, Eswarappa Prameela S, Izadi E and Rajagopalan J 2016 Capillary driven flow of polydimethylsiloxane in open rectangular microchannels Soft Matter 12 5818–23 [PubMed: 27301750]
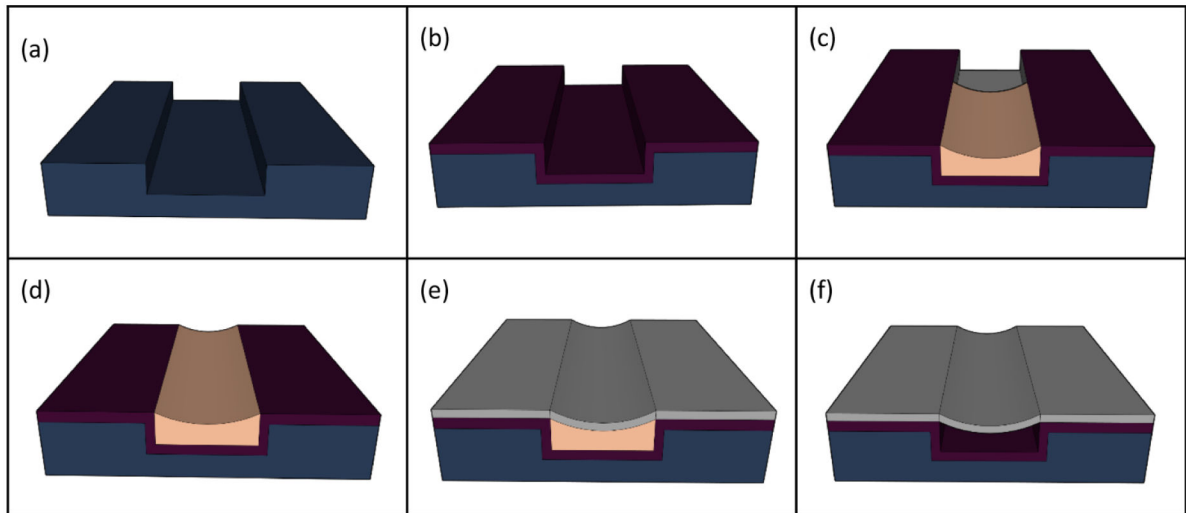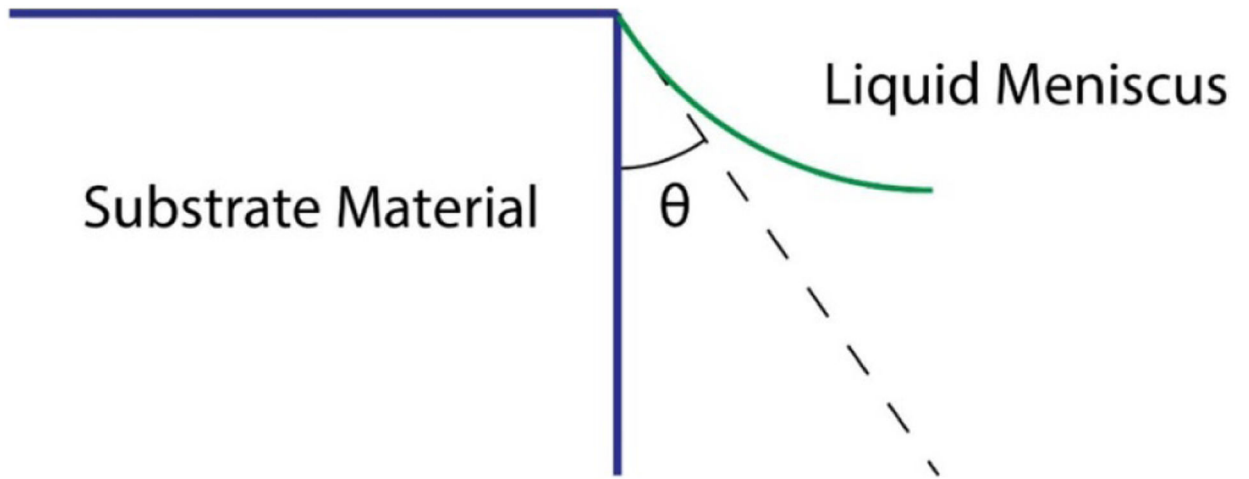
Figure 1.
Outline of fabrication process for natural meniscus formed membranes (a) Channel etched into silicon substrate. (b) A silicon dioxide layer is thermally grown on the entire wafer. (c & d) The channel is filled with SU8 2000.5 using spontaneous capillary flow. (e) PECVD silicon dioxide layer is deposited on wafer. (f) SU8 2000.5 is sacrificially etched, leaving a hollow channel.
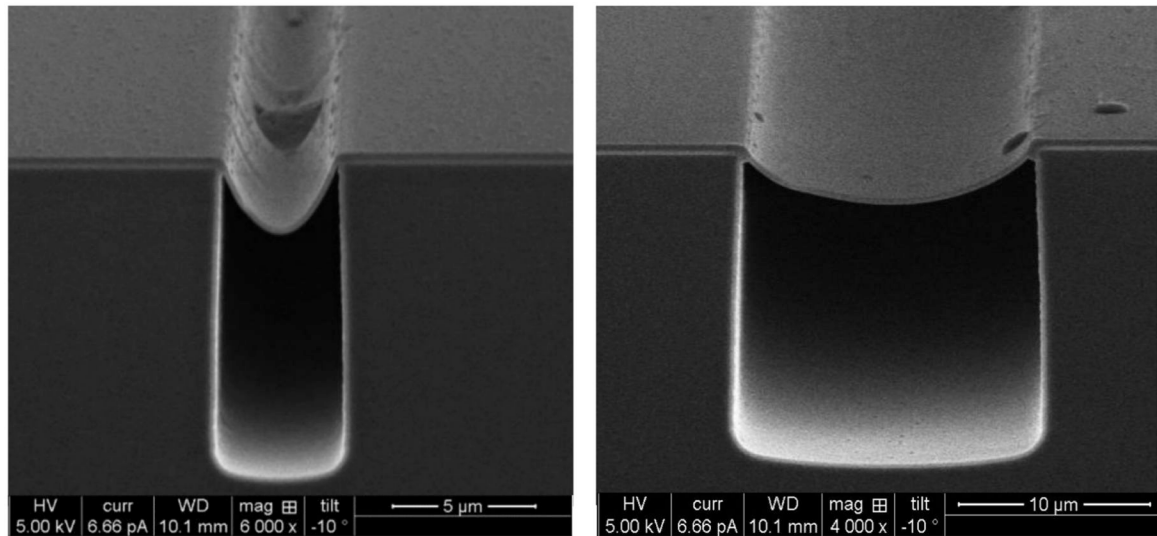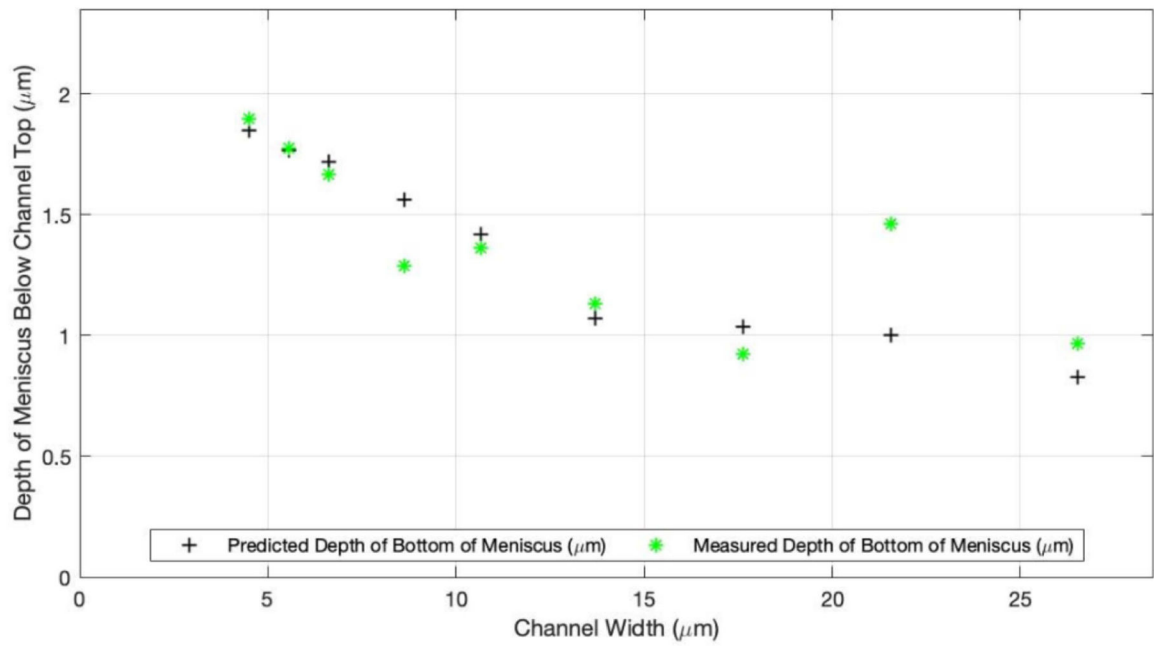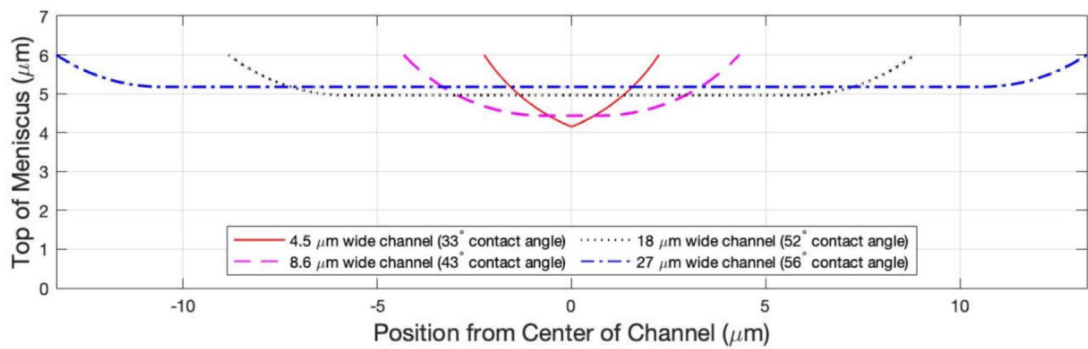
Figure 2.
SEM images of intact membranes suspended over microfluidic channels. Left: 200 nm thick membrane with a 3 μm width by 12 μm deep channel. Right: 200 nm thick membrane with a 7 μm width by 12 μm deep channel.

Figure 3.
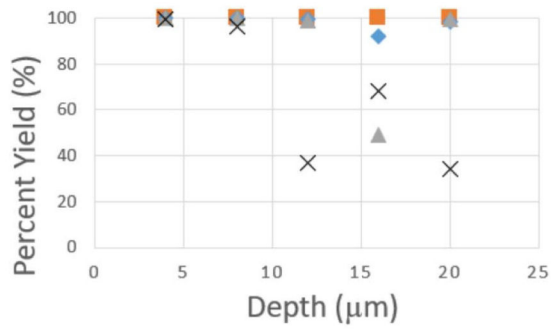Contact angle for a pinned liquid meniscus at a channel corner.
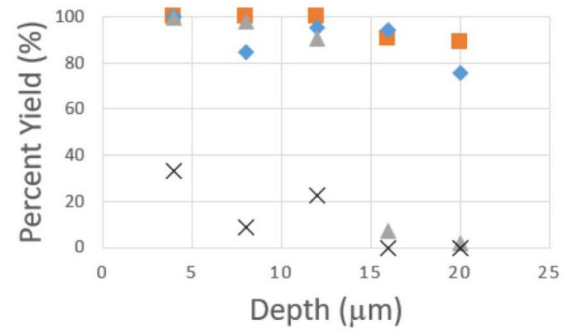
(a)

(b)

Figure 4.
(a) Predicted versus measured depth of bottom of meniscus (b) Model for the meniscus profile using measured channel widths and contact angles.
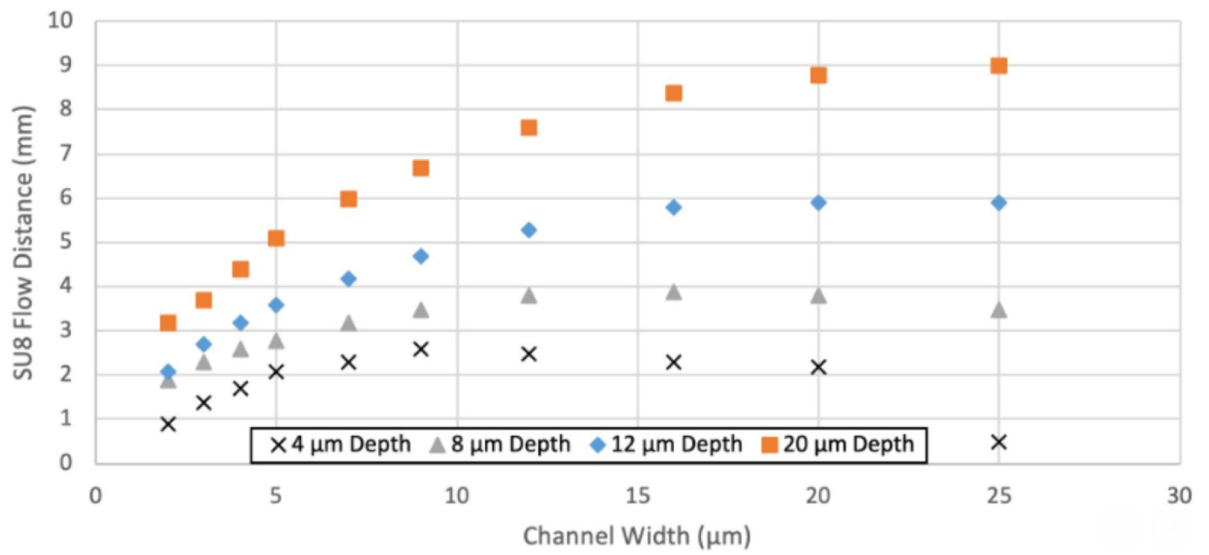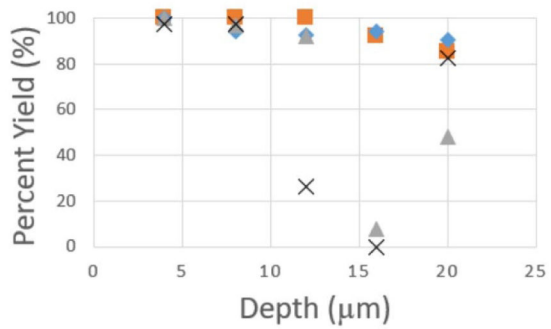
Figure 5.
Plot of SU8-2000.5 flow distance in microfluidic channels versus channel width for various depths. The SU8 was heated to 250 °C.
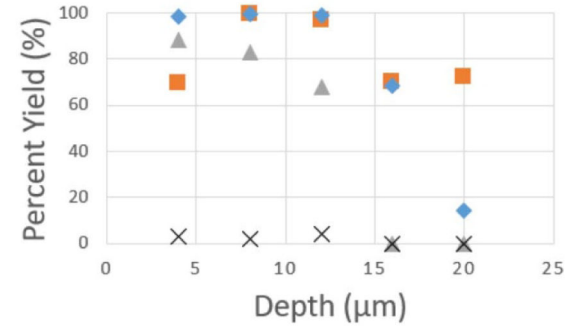
Figure 6.
Plot of depth versus average yield percentage for varying channel widths. (a) 4 μm wide channels; (b) 7 μm wide channels; (c) 12 μm wide channels; (d) 20 μm wide channels. Membrane thickness: ■ 200 (nm), ♦ 150 (nm), ▲ 100 (nm), × 50 (nm).